JPn Neuroscience

The Journal of Physiology

J Physiol 590.16 (2012) pp 4029–4044

Deficiency of sphingomyelin synthase-1 but not sphingomyelin synthase-2 causes hearing impairments in mice

Mei-Hong Lu[1], Makoto Takemoto[1], Ken Watanabe[2], Huan Luo[1], Masataka Nishimura[1], Masato Yano[3], Hidekazu Tomimoto[4], Toshiro Okazaki[5], Yuichi Oike[3] and Wen-Jie Song[1]

[1]*Department of Sensory and Cognitive Physiology, Graduate School of Medical Sciences, Kumamoto University, Kumamoto 860-0811, Japan*
[2]*Department of Bone and Joint Disease, National Center for Geriatrics and Gerontology, Aichi 474-8511, Japan*
[3]*Department of Molecular Genetics, Graduate School of Medical Sciences, Kumamoto University, Kumamoto 860-0811, Japan*
[4]*Department of Neurology, Mie University Graduate School of Medicine, Mie 514-8507, Japan*
[5]*Department of Hematology and Immunology, Kanazawa Medical University, Ishikawa 920-0293, Japan*

Key points

- Sphingomyelin (SM) is a structural component of plasma membrane and may participate in signal transduction. The role of SM metabolism in hearing remains controversial.
- Here we examined hearing in mice deficient of SM synthase-1 (SMS1) or SMS2, and show that only deficiency of SMS1 causes hearing loss.
- The hearing loss in SMS1 knockout mice is attributable at least in part to a reduction of endocochlear potential.
- The reduction of endocochlear potential is attributable at least in part to atrophy of the cochlear stria vascularis and its altered expression of K^+ channels.
- Our results establish that SMS1 is essential for normal inner ear function.

Abstract Sphingomyelin (SM) is a sphingolipid reported to function as a structural component of plasma membranes and to participate in signal transduction. The role of SM metabolism in the process of hearing remains controversial. Here, we examined the role of SM synthase (SMS), which is subcategorized into the family members SMS1 and SMS2, in auditory function. Measurements of auditory brainstem response (ABR) revealed hearing impairment in *SMS1*$^{-/-}$ mice in a low frequency range (4–16 kHz). As a possible mechanism of this impairment, we found that the stria vascularis (SV) in these mice exhibited atrophy and disorganized marginal cells. Consequently, *SMS1*$^{-/-}$ mice exhibited significantly smaller endocochlear potentials (EPs). As a possible mechanism for EP reduction, we found altered expression patterns and a reduced level of KCNQ1 channel protein in the SV of *SMS1*$^{-/-}$ mice. These mice also exhibited reduced levels of distortion product otoacoustic emissions. Quantitative comparison of the SV atrophy, KCNQ1 expression, and outer hair cell density at the cochlear apical and basal turns revealed no location dependence, but more macrophage invasion into the SV was observed in the apical region than the basal region, suggesting a role of cochlear location-dependent oxidative stress in producing the frequency dependence of hearing loss in *SMS1*$^{-/-}$ mice. Elevated ABR thresholds, decreased EPs, and abnormal KCNQ1 expression patterns in *SMS1*$^{-/-}$ mice were all found to be progressive

M-H. Lu and M. Takemoto contributed equally to this work.

DOI: 10.1113/jphysiol.2012.235846

with age. Mice lacking SMS2, however, exhibited neither detectable hearing loss nor changes in their EPs. Taken together, our results suggest that hearing impairments occur in *SMS1*$^{-/-}$ but not *SMS2*$^{-/-}$ mice. Defects in the SV with subsequent reductions in EPs together with hair cell dysfunction may account, at least partially, for hearing impairments in *SMS1*$^{-/-}$ mice.

(Resubmitted 2 May 2012; accepted after revision 25 May 2012; first published online 28 May 2012)
Corresponding author W.-J. Song: Department of Sensory and Cognitive Physiology, Graduate School of Medical Sciences, Kumamoto University, Kumamoto 860-0811, Japan. Email: song@kumamoto-u.ac.jp

Abbreviation ABR, auditory brainstem response; DAPI, 4,6-diamidino-2-phenylindole; DPOAE, distorted product of otoacoustic emission; EP, endocochlear potential; KO, knockout; PP, potassium potential; RT, room temperature; SM, sphingomyelin; SMS, sphingomyelin synthase; SPL, sound pressure level; SV, stria vascularis.

Introduction

Sphingolipids are important membrane structural components that participate in signal transduction (Hannun & Obeid, 2002; Merrill, 2002, Spiegel & Milstien, 2002). Accumulating evidence indicates that sphingolipids are involved in several neural functions, such as channel gating (Xu *et al.* 2008), synaptic transmission (Darios *et al.* 2009), and learning and memory (Dunbar *et al.* 1993; Inokuchi *et al.* 1997). Recently, several studies have suggested a role for sphingolipids in hearing. For example, knockout (KO) mice that are genetically devoid of ganglioside GM3 synthase exhibit complete hearing loss (Yoshikawa *et al.* 2009). Similarly, deficiency of the sphingosine 1-phosphate receptor $S1P_2$ also causes profound hearing loss (MacLennan *et al.* 2006; Herr *et al.* 2007; Kono *et al.* 2007).

Sphingomyelin (SM) is a major species of sphingolipids. The synthesis of SM from ceramide and phosphatidylcholine is mediated by SM synthase (SMS), which is subcategorized into the family members SMS1 and SMS2 (Huitema *et al.* 2004; Yamaoka *et al.* 2004; Tafesse *et al.* 2006). While SMS1 is localized in the Golgi apparatus, SMS2 is found in the plasma membrane in both neuronal (Kidani *et al.* 2012) and non-neuronal cells (Huitema *et al.* 2004). The expression of both enzymes has been studied at the organ level, and is found in a variety of organs including the brain (Huitema *et al.* 2004; Yang *et al.* 2005). Recently, it has been shown that SMS1 deficiency impairs endocrine (Yano *et al.* 2011) and immune (Dong *et al.* 2012) functions, while SMS2 deficiency ameliorates high fat diet-induced obesity (Li *et al.* 2011; Mitsutake *et al.* 2011), attenuates lipopolysaccharide-induced lung injury (Gowda *et al.* 2011), reduces atherosclerosis (Liu *et al.* 2009), and reduces the expression of drug transporters in the brain (Zhang *et al.* 2011). SM is hydrolysed into phosphocholine and ceramide by sphingomyelinase (Jung *et al.* 2000; Hannun & Obeid, 2002). A previous study reported that mutations of sphingomyelinase cause Niemann–Pick disease, which is associated with hearing loss (Konagaya *et al.* 1989). A recent study, however, reported normal auditory brainstem responses (ABR) in every subject in a sample of seven Niemann–Pick patients with sphingomyelinase-deficiency (Mihaylova *et al.* 2007). The relationship between SM metabolism and hearing thus requires further investigation. Here, we addressed this issue by examining hearing in SMS1- and SMS2-deficient mice. Our results revealed that while *SMS1*$^{-/-}$ mice exhibited progressive hearing loss in the low frequency range, the hearing abilities of *SMS2*$^{-/-}$ mice were no different from their *SMS2*$^{+/+}$ controls. In addition, we observed a decrease in the endocochlear potential (EP), atrophy of the stria vascularis (SV), and altered expression of the KCNQ1 channel in the SV in the inner ear of *SMS1*$^{-/-}$ mice. These findings may at least partially account for the hearing impairments in these animals. Moreover, the results also revealed a greater increase of macrophage invasion into the SV at the apical region compared with the basal region of the cochlea in *SMS1*$^{-/-}$ mice, possibly explaining the frequency dependence of hearing loss in the animals.

Methods

Genotyping

All experiments were approved by the Committee for Animal Experiments of Kumamoto University, and were carried out in accordance with the Guidelines for Animal Experimentation of Kumamoto University. As we reported previously, SMS1- and SMS2-deficient mice were generated using D3 stem cells, and backcrossed with the C57BL/6 strain for three generations (SMS1 KO) or 10 generations (SMS2 KO) (Mitsutake *et al.* 2011; Yano *et al.* 2011). Thus, all mice used here were 129/Sv-C57BL/6 mixed-background littermates from heterozygote crosses. Although SMS1 KO mice suffer from postnatal mortality due to sudden death (Yano *et al.* 2011), all mice used in the current study appeared healthy.

Exon 2 of the *SMS1* gene was replaced by a neo cassette, and PCR-based genotyping was performed using primer pairs that target either exon 2 or the neo cassette (Yano *et al.* 2011). SMS2-deficient mice were generated by targeting

exon 2 of *SMS2* and genotyped in a strategy similar to that used for the SMS1-deficient mice (Mitsutake *et al.* 2011). The procedures used for DNA extraction, primer sequences, and PCR reaction conditions to complete the genotyping followed the procedures described by Yano *et al.* (2011) and Mitsutake *et al.* (2011).

ABR measurements

All mice were anaesthetized with a mixture of ketamine (72 mg (kg weight)$^{-1}$) and xylazine (7.2 mg kg^{-1}). An adequate degree of anaesthesia was verified by the absence of reflexes in response to toe pinches. ABRs to the acoustic stimuli were recorded as the potential difference between the left ear lobe and the vertex, using subcutaneous wire electrodes. Click stimuli (one-cycle sine wave, 0.1 ms duration) and tone bursts (4, 6, 8, 16, 24 and 32 kHz; 1 ms rise/fall cosine ramp, 1 ms plateau) were generated digitally at a sampling rate of 97.7 kHz and delivered via a speaker positioned 10 cm from the ear. Sound stimuli were first applied at 20–80 dB sound pressure levels (SPLs) with 10 dB steps between the levels to find the gross response threshold. The SPL was then finely adjusted from the gross threshold at 3 dB steps to determine the precise ABR threshold. The ABR threshold was defined as the lowest sound intensity at which the signal exceeded three times the standard deviation (SD) of baseline noise (baseline: 10 ms recording before stimulus onset). Acoustic stimulus generation and delivery were performed using Tucker-Davis Technologies (Alachua, FL, USA) System III hardware and software, as reported previously (Nishimura *et al.* 2007). The SPL was calibrated either with a Brüel & Kjær sound level meter (type 2610 with a model 4191 microphone, Brüel & Kjær, Nærum, Denmark) or a portable sound level meter (LA-5111, Ono Sokki, Kanagawa, Japan) which reported dB values close to those reported by the Brüel and Kjær meter (±2 dB). For each stimulus condition, 3000 trials with an inter-trial interval of 0.1 s were conducted. The signal was amplified 100,000-fold, filtered (15 Hz–10 kHz), and averaged across the trials. All data acquisition and analyses were conducted with custom-made software. The body temperature was maintained at 38 ± 0.3°C. Recordings were taken in a sound-attenuating chamber.

Otoacoustic emissions measurement

All mice were anaesthetized as described above, and their pinnae were removed. A probe microphone/speaker system with two speaker ports (ER10B+, Etymotic Research, Inc., Elk Grove Village, IL, USA.) was fitted tightly into the ear canal. Two closed-field speakers (EC-1, Tucker-Davis Technologies, Inc.) were connected to the ER10B+ ports. Two primary tones (1 s duration with 20 ms rise/fall cosine ramp; $f_2/f_1 = 1.22$, f_2 varied at a one-fourth octave step from 4 to 29 kHz) were generated as described above, and routed separately to the two EC1 speakers, at SPL1 = 75 dB and SPL2 = 65 dB. The SPL was calibrated in a 0.1 ml coupler (Polesskaya *et al.* 2010), using a Brüel and Kjær 1/4″ pressure field microphone (model 4938), which has a flat frequency response from 4 Hz to 70 kHz. The calibration was conducted for primary tones and all distortion product of otoacoustic emission (DPOAE) components. The DPOAE response from the ER10B+ microphone was amplified by 20 dB and digitized at 150 kHz using an A/D converter (PCI-MIO-16E-1, National Instruments, Inc., Austin, TX, USA). All data acquisition and analysis was performed using custom software written in Matlab (The Mathworks, Inc., Natick, MA, USA). The recordings were repeated 10 times at an interval of 20 s and averaged in the time domain. The noise level was estimated by averaging three adjacent frequency bins that were above and below the DPOAE frequency.

EP and K^+ concentration measurements

EP and K^+ concentrations were measured simultaneously using a double-barrel electrode in mice anaesthetized as described above, following previously reported methods (Nin *et al.* 2008). Briefly, one barrel was silanized with dimethyldichlorosilane (5% in toluene), filled with a K^+ exchanger solution (IE190, WPI, Sarasota, FL, USA) in the tip, and back-filled with a 150 mM KCl solution, to measure the K^+ concentration. The other barrel was filled with a 150 mM NaCl solution to measure the EP. Each barrel was connected to a separate channel of a high-impedance dual channel electrometer (FD223a, WPI). A reference AgCl electrode was placed in the neck muscle. Signals from the electrometer were amplified and digitized at 100 Hz using an A/D converter (NI9205, National Instruments, Inc.). All data acquisition and analysis was performed using custom software written in Matlab. For recording, the tympanic bulla was removed through the lateral approach. A small hole was carefully made in the middle turn of the cochlea to expose the spiral ligament, using a fine drill. The electrode was advanced through the spiral ligament, and a sudden increase of potential signalled the entrance of the microelectrode tip into the endolymph. Recordings were used for analysis only when the EP was stable for >1 min. Before and immediately after each experiment, the ion exchanger-filled microelectrode was calibrated using a series of KCl solutions that ranged in concentration from 5 mM to 160 mM. The results of the calibration were fitted with the Nicolski equation in the form: $V = V_0 + S \times \log(a[K^+] + Aa[Na^+])$, where V is K^+ potential, V_0 is offset, S is slope, a is activity coefficient, and A is ion selectivity. Only electrodes with a slope greater than 55 mV per 10-fold increase in ionic strength were used for recording. Recordings were used for analysis only when

the difference in the values of the slopes obtained from the calibrations before and after the recording was less than 2%. The endolymph K^+ concentration was determined from the calibration curve obtained after each recording, using the voltage difference between the potential from the ion exchanger-filled barrel and the EP.

Histochemistry

Animals were transcardially perfused with 4% paraformaldehyde in 0.1 M phosphate buffer under deep anaesthesia (ketamine 100 mg kg^{-1} and xylazine 10 mg kg^{-1}). The inner ear at both sides was then harvested and fixed in 4% paraformaldehyde for an additional 1–2 days, before decalcification with 10% ethylenediaminetetraacetic acid for 2 days at room temperature (RT) or 3 days at 4°C. In each animal, one cochlea was sectioned, whereas the other cochlea was used for flat-mount tissue preparations. For sectioning, the decalcified cochlea was cryoprotected in a series of sucrose in phosphate buffered saline (PBS) solutions, and sectioned at 6 μm thickness with a cryostat. For flat-mount preparations, the cochlea was dissected into apical, middle and basal turns. The basilar membrane with cochlear hair cells was then separated from the cochlear lateral wall tissue which included the SV. The tissues were then cut into several pieces to allow them to be flattened on a glass slide.

F-actin staining was performed to visualize cochlear hair cells and marginal cells of the SV. Pieces of cochlear tissues were incubated in rhodamine-conjugated phalloidin (Invitrogen R415, 1:200) in PBS with 0.1% Triton X-100 for 30 min at RT.

For KCNQ1 immunohistochemistry, cochlear sections were blocked with PBS containing 5% normal donkey serum and 0.1% Triton X-100 for 1 h at RT. The sections were then incubated with a goat anti-KCNQ1 polyclonal antibody (Santa Cruz sc-10646, 1:200; Santa Cruz Biotechnology, Inc., Santa Cruz, CA, USA) overnight at 4°C, followed by reaction with an Alexa Fluor 488-conjugated donkey anti-goat IgG (Invitrogen A11055, 1:500) for 1–2 h at RT. All sections were counterstained with 4,6-diamidino-2-phenylindole (DAPI).

Western blotting

Three-month-old *SMS1*$^{+/+}$ and *SMS1*$^{-/-}$ mice (10 of each genotype) were decapitated under deep anaesthesia as described above and the cochlea was harvested. SV fractions from each genotype were dissected in cold PBS, and lysed with a sample buffer (50 mM Tris-HCl, pH 6.8, 10% glycerol, 2% SDS, 0.1% bromophenol blue, and 6% 2-mercaptoethanol) overnight at 4°C. Samples were not subjected to heat treatment prior to Western blot analysis to avoid degradation. Other methods of Western blot analysis followed previously described procedures (Yamagata *et al.* 2011), except that the anti-KCNQ1 antibody was from Santa Cruz (sc-10646, 1:300) and that glyceraldehyde-3-phosphate dehydrogenase (GAPDH) was also analysed as a control protein using an antibody from Sigma (G9545, 1:10,000). Proteins were visualized using ECL western blotting detection reagents (GE Healthcare) and images were obtained and analysed with a LAS 4000 imaging system (Fuji Film, Tokyo, Japan).

Data analyses

To quantify the apical membrane area size of the strial marginal cells, phalloidin-stained compartment boundaries were determined using NIH ImageJ software and manually verified. The area sizes were then measured using the software. For evaluating pigmentations in the SV, brightfield images of flat-mount SV tissues were acquired, converted into 8-bit images, and binarized after subtracting the background noise, again using ImageJ software. The percentage of total area of binarized signals, i.e. the pigmented area, to the area of SV was calculated and compared between *SMS1*$^{-/-}$ and *SMS1*$^{+/+}$ mice, at the apical and basal levels of the cochlea. For evaluating atrophy of the SV, the SV width (width along the base-to-apex direction) was measured as the distance between the two points of SV, where its thickness decreased to half of the maximum, along the SV surface; the ratio of the SV width to the width of the lateral wall in the scala media was then calculated. The width of the lateral wall was measured as the distance between its two ends, defined by the Reissner's membrane and the basilar membrane, respectively, along the lateral wall surface in the scala media. KCNQ1 expression at the apical surface of SV was evaluated by the ratio of KCNQ1-positive length to the width of SV.

All data are described either as means ± standard error of the mean (SEM) (Fig. 1, Fig. 3, and Fig. 6) or as means ± SD (Fig. 2 and Fig. 4–5). Student's *t* test was used to test for group differences. Differences were considered statistically significant if $P < 0.05$.

Results

ABR tests

SMS1- and SMS2-deficient mice were generated and genotyped as reported previously by our group (Mitsutake *et al.* 2011; Yano *et al.* 2011). To test hearing in these mice, we examined the ABR threshold using a click stimulus. As shown in Fig. 1*A*, and in agreement with previous reports (Yoshikawa *et al.* 2009), ABRs in mice occurred 1–6 ms

after stimulus onset. The ABR threshold was defined as the lowest SPL required to induce an ABR exceeding three times the SD of baseline noise (see Methods). As shown in Fig. 1*A*, the ABR threshold in the $SMS1^{-/-}$ mouse was elevated compared with the threshold in the $SMS1^{+/+}$ mouse. Figure 1*B* shows the ABR threshold results in $SMS1^{-/-}$ animals at 1 month, 3 months, and 6 months of age and in $SMS2^{-/-}$ mice at 3 months of age. The ABR threshold in the $SMS1^{-/-}$ mice was significantly higher than that in age-matched $SMS1^{+/+}$ mice, at all ages ($P < 0.01$). There was also a clear elevation of ABR threshold in $SMS1^{-/-}$ mice that were 1–3 months of age ($P < 0.01$). In contrast, $SMS2^{-/-}$ mice exhibited low ABR thresholds that were not significantly different from those of their $SMS2^{+/+}$ control ($P > 0.05$; Fig. 1*B*, right end). These results clearly show that $SMS1^{-/-}$ mice exhibited hearing impairments, whereas $SMS2^{-/-}$ mice did not. Moreover, the hearing loss in $SMS1^{-/-}$ mice showed an age-related progression.

To test the frequency dependence of hearing loss in $SMS1^{-/-}$ mice, we examined the ABR threshold with tones of different frequencies. As shown in Fig. 1*C–E*, hearing impairments occurred at lower frequencies for all age groups tested. At 1 month of age, hearing loss was most prominent at 4 kHz, whereas at 3 and 6 months the most severe hearing loss occurred at 8 kHz (Fig. 1*C–E*). We also examined the frequency dependence of the ABR threshold in $SMS2^{-/-}$ mice, and again found no difference from their $SMS2^{+/+}$ controls at any frequency (Fig. 1*F*), consistent with observations using click stimulation.

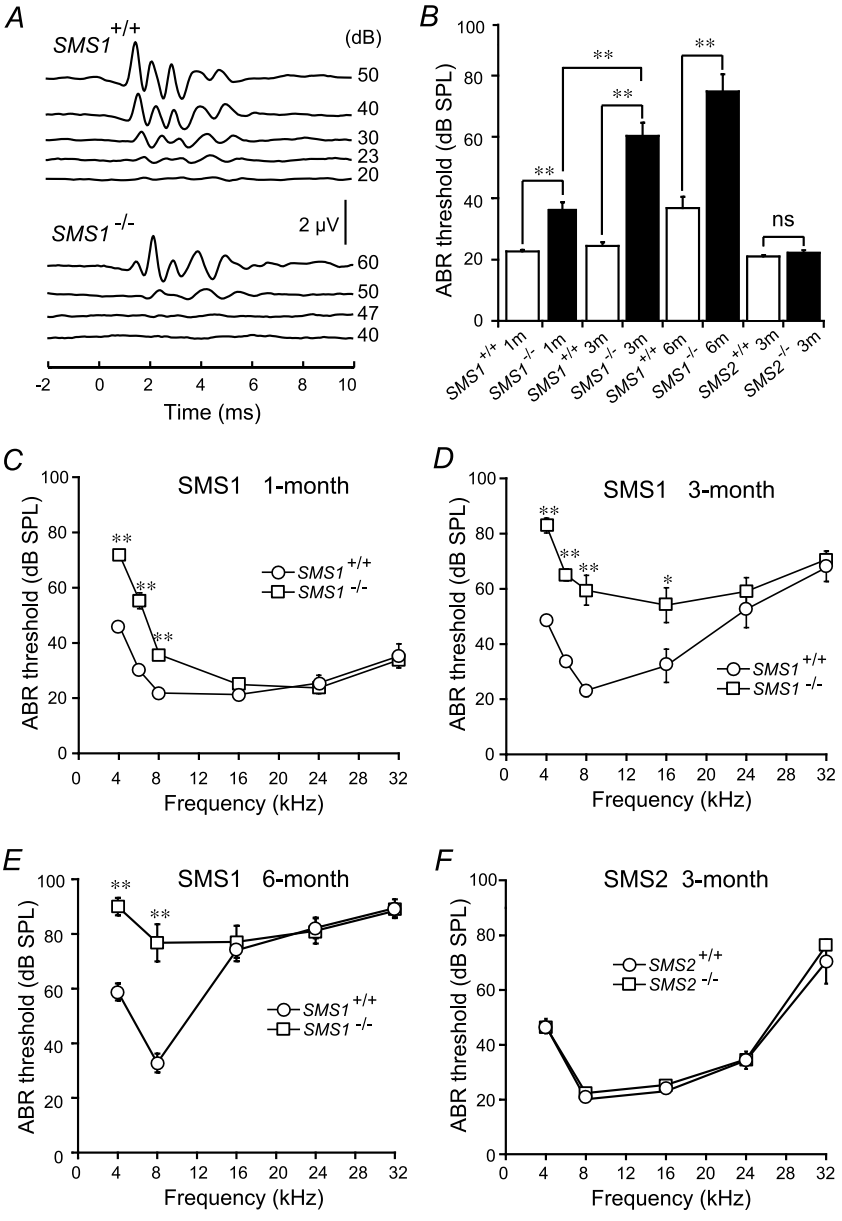

Figure 1. ABR analyses
A, representative click-evoked ABR waveforms from an $SMS1^{+/+}$ mouse (upper trace group) and an $SMS1^{-/-}$ mouse (lower trace group), both at 3 months of age. The voltage calibration scale applies to all recordings. *B*, ABR thresholds in response to a click stimulus in 1-month-old $SMS1^{+/+}$ ($n = 18$) and $SMS1^{-/-}$ ($n = 14$) mice, 3-month-old $SMS1^{+/+}$ ($n = 19$) and $SMS1^{-/-}$ ($n = 17$) mice, 6-month-old $SMS1^{+/+}$ ($n = 9$) and $SMS1^{-/-}$ ($n = 6$) mice, and 3-month-old $SMS2^{+/+}$ ($n = 6$) and $SMS2^{-/-}$ ($n = 6$) mice. *C*, comparison of ABR thresholds in response to tones of different frequencies in 1-month-old $SMS1^{+/+}$ ($n = 4$ for 6 kHz, $n = 11$ for other frequencies) and $SMS1^{-/-}$ ($n = 4$ for 6 kHz, $n = 9$ for other frequencies) mice. *D*, comparison of ABR thresholds in response to tones of different frequencies in 3-month-old $SMS1^{+/+}$ ($n = 4$ for 6 kHz, $n = 14$ for other frequencies) and $SMS1^{-/-}$ ($n = 4$ for 6 kHz, $n = 12$ for other frequencies) mice. *E*, comparison of ABR thresholds in response to tones of different frequencies in 6-month-old $SMS1^{+/+}$ ($n = 9$) and $SMS1^{-/-}$ ($n = 8$) mice. *F*, comparison of ABR thresholds in response to tones of different frequencies in 3-month-old $SMS2^{+/+}$ ($n = 6$) and $SMS2^{-/-}$ ($n = 6$) mice. ns: not significant. $^{*}P < 0.05$, $^{**}P < 0.01$. Asterisk conventions apply to all figures.

Because SM is also a component of axonal myelin sheath, changes may also be expected in the conduction velocity of axons in the KO mice. As a rough estimate of conduction time, we measured the interval from the first peak to the fifth peak in the ABR waveform in response to a click stimulation at 60 dB. The interval was 3.19 ± 0.12 ms in $SMS1^{+/+}$ mice ($n = 8$), 3.32 ± 0.07 ms in $SMS1^{-/-}$ mice ($n = 9$), 3.29 ± 0.04 ms in $SMS2^{+/+}$ mice ($n = 6$), and 3.33 ± 0.06 ms in $SMS2^{-/-}$ mice ($n = 6$) (all at 3 months of age). No significant differences were found between these groups ($P > 0.05$).

Cochlear function in the KO mice

The elevation of the ABR threshold in $SMS1^{-/-}$ mice means that the SPL required to induce the first peak of the ABR response, which reflects cochlear activity, was also elevated (see Fig. 1*A*). This finding suggests dysfunction of the cochlea, consistent with our observation that *SMS1* mRNA was expressed in the cochlea of $SMS1^{+/+}$ mice (Fig. S1). Because $SMS1^{-/-}$ mice were not completely deaf (Fig. 1), we suspected that mechanisms in the cochlea that enhance cochlear sensitivity may be impaired in these mice. We therefore first examined the EP and endolymph K^+ concentration, then otoacoustic emissions in the $SMS1^{-/-}$ mice.

We used a double-barrelled microelectrode to examine EPs and endolymph K^+ concentrations at the same time (Fig. 2*A*), in animals across different ages. As shown in Fig. 2*B* and *C*, the EP in the $SMS1^{+/+}$ mice exhibited a value close to 100 mV (98.0 ± 4.5 mV, $n = 10$, at 1 month of age; 96.1 ± 5.5 mV, $n = 8$, at 3 months of age; and 97.7 ± 6.7 mV, $n = 12$, at 6 months of age; no significant difference was found among these groups; $P > 0.05$), in agreement with previous reports in wild-type animals (Kitajiri *et al.* 2004; Yoshikawa *et al.*

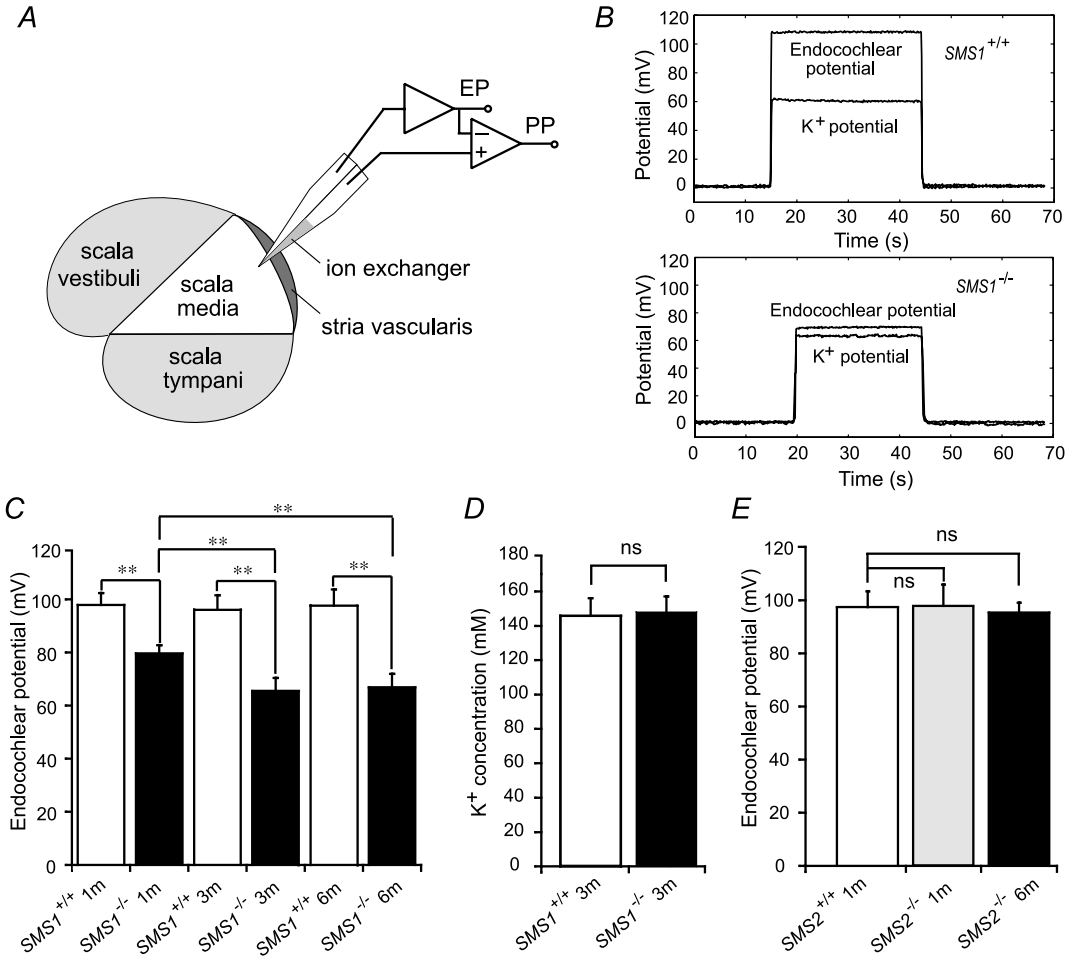

Figure 2. Measurement of the EPs and endolymph K^+ concentrations
A, a schematic diagram illustrating the method for simultaneous recording of the EPs and K^+ potentials (PPs). *B*, representative recordings of EPs and PPs from the cochlea of an $SMS1^{+/+}$ mouse and an $SMS1^{-/-}$ mouse, both at 3 months of age. *C*, summary of EPs recorded from age-matched $SMS1^{+/+}$ and $SMS1^{-/-}$ mice. *D*, comparison of K^+ concentration in 3-month-old $SMS1^{+/+}$ and $SMS1^{-/-}$ mice. *E*, EPs in $SMS2^{+/+}$ and $SMS2^{-/-}$ mice. ns: not significant.

2009). The EPs in $SMS1^{-/-}$ mice at 1 month of age (79.7 ± 4.5 mV, $n = 8$), 3 months of age (65.5 ± 4.9 mV, $n = 10$), and 6 months of age (68.7 ± 4.5 mV, $n = 8$) were all found to be significantly reduced compared with age-matched $SMS1^{+/+}$ controls (Fig. 2*B* and *C*; $P < 0.01$). The potentials in 3-month-old and 6-month-old $SMS1^{-/-}$ mice were also significantly lower than that of the 1-month-old animals (Fig. 2*C*; $P < 0.01$).

In accord with previous reports on wild-type animals (Kitajiri *et al.* 2004; Yoshikawa *et al.* 2009), the K^+ concentration in the endolymph of $SMS1^{+/+}$ mice was 144.4 ± 10.2 mM (Fig. 2*D*; $n = 11$). The K^+ concentrations in the endolymph of age-matched $SMS1^{-/-}$ mice were found to have similar values (146.9 ± 9.0 mM, $n = 9$, $P > 0.05$; Fig. 2*D*).

EPs in $SMS2^{-/-}$ mice either at 1 month of age (98.0 ± 8.0 mV, $n = 6$) or at 6 months of age (95.4 ± 3.8 mV, $n = 8$) were not significantly different from those in the $SMS2^{+/+}$ mice (97.3 ± 6.1 mV, $n = 6$ at 1 month; $P > 0.05$; Fig. 2*E*). These EP values were also not significantly different from those in the $SMS1^{+/+}$ mice ($P > 0.05$).

We examined otoacoustic emissions in the frequency range of 4 kHz to 29 kHz by fitting a probe microphone/speaker system to the ear canal. Figure 3*A* shows an example of a DPOAE measurement from a 3-month-old $SMS1^{+/+}$ mouse. Application of two primary tones of frequencies f_1 and f_2 ($f_2/f_1 = 1.22$) induced distortion components of $2f_1 - f_2$, $3f_1 - 2f_2$, and $4f_1 - 3f_2$, among which the cubic component $2f_1 - f_2$ had the largest magnitude (Fig. 3*A*). We compared the $2f_1 - f_2$ component measured at different frequencies in KO and control animals (Fig. 3*B*). The component was significantly smaller in $SMS1^{-/-}$ mice in the middle frequency range (8–16 kHz) than in $SMS1^{+/+}$ controls ($P < 0.01$, Fig. 3*B*).

Cochlear histology

The observation of smaller EPs in $SMS1^{-/-}$ mice, as described above, suggests alterations in the cochlear SV of the $SMS1^{-/-}$ mice because the SV is known to play a vital role in the generation of EPs (Wangemann, 2002; Hibino *et al.* 2010). Histological examination of the cochlea indeed revealed alterations in $SMS1^{-/-}$ mice. Figure 4*A* and *B* show a hematoxylin and eosin-stained section through the middle turn of the cochlea in a 3-month-old $SMS1^{+/+}$ mouse, and an age-matched $SMS1^{-/-}$ mouse, respectively. Although there was no clear change in the organ of Corti, hair cell, or spiral ganglion, atrophy of the SV was observed in the $SMS1^{-/-}$ mouse. As shown in Fig. 4*B*, the SV at regions towards the apical end and the basal end appeared much thinner in $SMS1^{-/-}$ mice compared with $SMS1^{+/+}$ controls (Fig. 4*B*, arrows). Because previous studies have established a place-frequency map in the mouse cochlea (Müller *et al.* 2005), we quantitatively examined SV atrophy at the apical, middle and basal turns of the cochlea to explore cochlear mechanisms for the frequency dependence of hearing loss in $SMS1^{-/-}$ mice. Because the ends of SV appeared vague in cross sections (Fig. 4*A* and *B*), we defined the ends of SV as the point at which SV thickness reduced to half of its maximum, and defined the width of SV (width in the base-to-apex direction) as the distance between the defined ends, along the SV surface. As shown in Fig. 4*C*, the SV width was significantly shorter in $SMS1^{-/-}$ mice than in age-matched $SMS1^{+/+}$ controls, at all cochlear locations, and for both 3-month-old and

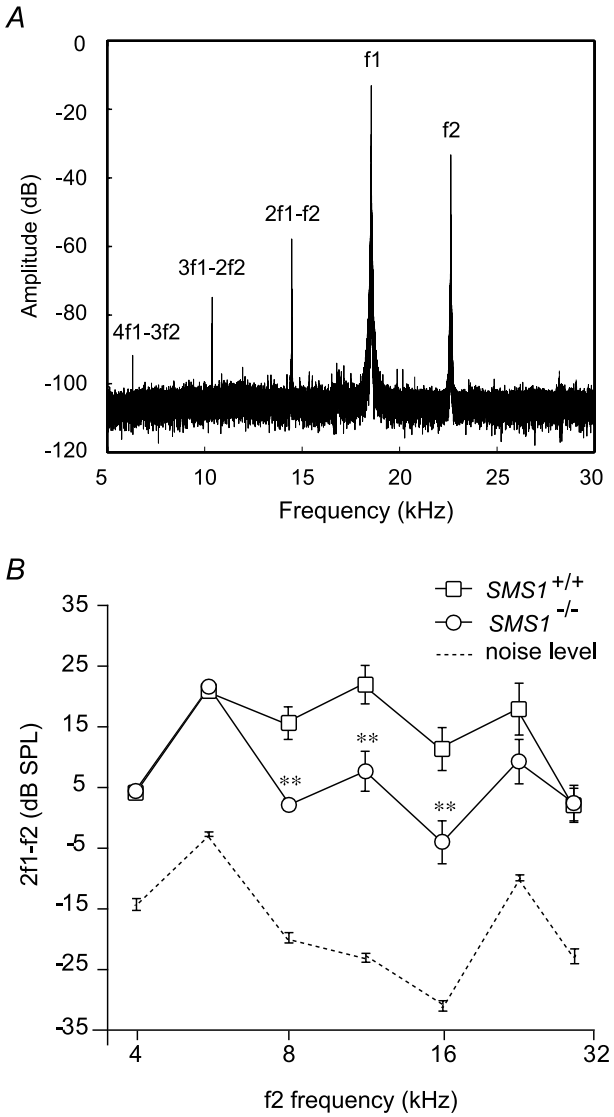

Figure 3. DPOAE test results in $SMS1^{+/+}$ and $SMS1^{-/-}$ mice at 3 months of age
A, a representative DPOAE result from an $SMS1^{+/+}$ mouse. *B*, frequency dependence of the $2f_1 - f_2$ component in 3-month-old $SMS1^{+/+}$ ($n = 12$) and $SMS1^{-/-}$ ($n = 17$) mice.

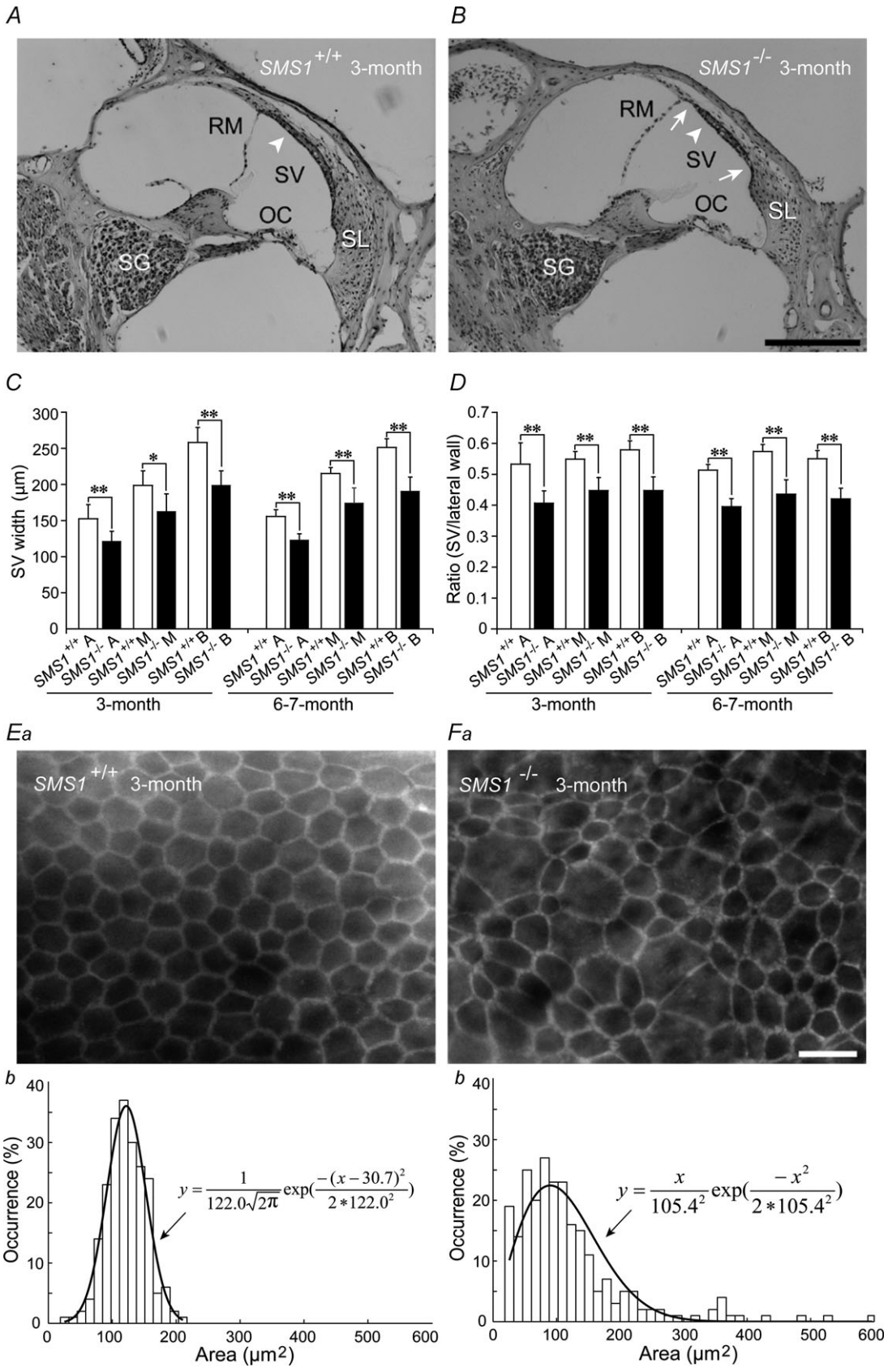

6- to 7-month-old animals. To test cochlear location dependence, we normalized the SV width to the width of the lateral wall, measured between its two ends defined by the Reissner's membrane and the basilar membrane, respectively. As shown in Fig. 4*D*, although the ratio was significantly smaller in the KO animals than $SMS1^{+/+}$ controls at all cochlear locations and at both ages, we found no difference between cochlear locations. The reduction in the ratio in the KO animals was attributable to reduction in SV width, because the lateral wall width was independent of genotype (width in μm in 3-month-old mice: apical: $SMS1^{+/+}$ (286.4 ± 15.8, $n = 6$), $SMS1^{-/-}$ (299.2 ± 18.7, $n = 6$), $P > 0.05$; middle: $SMS1^{+/+}$ (361.5 ± 32.8, $n = 6$), $SMS1^{-/-}$ (362.5 ± 25.0, $n = 6$), $P > 0.05$; basal: $SMS1^{+/+}$ (445.7 ± 24.0, $n = 5$), $SMS1^{-/-}$ (445.8 ± 29.0, $n = 6$), $P > 0.05$. 6- to 7-month-old: apical: $SMS1^{+/+}$ (302.9 ± 9.8, $n = 4$), $SMS1^{-/-}$ (311.5 ± 7.9, $n = 5$), $P > 0.05$; middle: $SMS1^{+/+}$ (375.1 ± 5.6, $n = 4$), $SMS1^{-/-}$ (399.9 ± 11.6, $n = 5$), $P > 0.05$; basal: $SMS1^{+/+}$ (456.8 ± 20.0, $n = 4$), $SMS1^{-/-}$ (453.3 ± 17.8, $n = 5$), $P > 0.05$).

In addition to the shrinkage of SV in the $SMS1^{-/-}$ mice, F-actin staining with phalloidin revealed disorganization of marginal cells of the SV in these mice. At the SV surface, phalloidin labels the tight junctions connecting marginal cells and thus reveals the shape and size of the apical membrane of individual marginal cells (Jabba *et al.* 2006). As shown in Fig. 4*Ea*, marginal cells at the middle turn of the cochlea in $SMS1^{+/+}$ animals at 3 months of age exhibited polygonal shapes, but the size of the cells appeared rather uniform across the epithelium. In contrast, marginal cells in age-matched $SMS1^{-/-}$ mice showed marked variation in their sizes (Fig. 4Fa). For a quantitative comparison, we measured apical membrane area size in both $SMS1^{-/-}$ and $SMS1^{+/+}$ mice using NIH ImageJ software. The mean apical membrane area size was 122.0 μm^2 with an SD of 30.7 μm^2 (210 cells from three animals) in control mice, and 118.9 μm^2 with an SD of 90.1 μm^2 (239 cells from three animals) in $SMS1^{-/-}$ mice. The sizes in the control animals could be well fitted with a Gaussian function (Fig. 4*Eb*; $P < 0.05$, χ^2 test). In contrast, the distribution of the sizes in $SMS1^{-/-}$ mice was strongly skewed towards the right and could not be fitted with a Gaussian function (Fig. 4*Fb*; $P > 0.05$, χ^2 test), but could be approximated with a Rayleigh function with a scale parameter of 105.4 (Fig. 4*Fb*; $P < 0.05$, χ^2 test). Although we did not compare marginal cell size at different cochlear locations in a quantitative manner, the change in the KO animals appeared to be largely independent of cochlear location. At 6 months of age, although there was no obvious change in $SMS1^{+/+}$ animals, marginal cell boundaries defined by phalloidin staining in $SMS1^{-/-}$ mice became vague (data not shown).

The histological results described above may explain in part the reduction in EP, but do not appear to explain the frequency dependence of hearing loss in $SMS1^{-/-}$ mice. To further explore the mechanisms underlying the frequency dependence of hearing loss in the KO mice, we examined the density of outer hair cells. The abnormalities of DPOAE in $SMS1^{-/-}$ mice described in Fig. 3 also suggest alterations of the hair cells in these animals. Loss of hair cells in $SMS1^{-/-}$ mice, however, was limited, and we found no significant difference in outer hair cell density between $SMS1^{-/-}$ and $SMS1^{+/+}$ mice, at either the apical turn or the basal turn of the cochlea, and at either 3 months of age or at 6–7 months of age (Fig. S2).

KCNQ1 expression in the strial marginal cells

The attenuated EPs in $SMS1^{-/-}$ mice described above may partially account for the hearing impairments in these animals, and the abnormalities of the SV in $SMS1^{-/-}$ mice may partially explain the attenuated EPs. To further explore the mechanisms underlying the attenuated EPs and the frequency dependence of hearing loss in $SMS1^{-/-}$ mice, we examined the expression of KCNQ1, a voltage-dependent potassium channel in the SV that plays an essential role in controlling EPs (Wangemann, 2002; Hibino *et al.* 2010). Immunostaining of KCNQ1 in the $SMS1^{+/+}$ mouse cochlea (3 months old) revealed that the channel was expressed exclusively on the apical surface of strial marginal cells (Fig. 5*A*, green), in accord with previous reports in wild-type animals (Sakagami *et al.* 1991; Jabba *et al.* 2006). Figure 5*B*

Figure 4. Morphological abnormalities of the SV in $SMS1^{-/-}$ mouse cochlea *A* and *B*, haematoxylin- and eosin-stained cochlear sections at the middle turn in 3-month-old $SMS1^{+/+}$ (*A*) and $SMS1^{-/-}$ (*B*) mice. Arrowhead points to the SV. Note the shrinkage of the SV at locations indicated by the arrows in the $SMS1^{-/-}$ mice (*B*). *C* and *D*, summary of SV width (*C*) and the ratio of SV width to lateral wall width (*D*) at the apical (A), middle (M) and basal (B) turns of cochleae from $SMS1^{+/+}$ and $SMS1^{-/-}$ mice at 3 months of age ($n = 6$ for each genotype), and at 6–7 months of age ($SMS1^{+/+}$, $n = 4$; $SMS1^{-/-}$, $n = 5$). *Ea* and *Fa*, phalloidin-stained strial marginal cells in flat-mount cochlear lateral wall preparations. *Eb* and *Fb*, histograms of marginal cell apical membrane area size in age-matched $SMS1^{+/+}$ (*Eb*, 210 cells from 3 animals) and $SMS1^{-/-}$ (*Fb*, 239 cells from 3 animals) mice. The size in $SMS1^{+/+}$ mice was fitted with a Gaussian function (*Eb*, $P < 0.05$, χ^2 test), and the size in $SMS1^{-/-}$ mice was fitted with a Rayleigh function (*Fb*, $P < 0.05$, χ^2 test). Abbreviations: OC, the organ of Corti; RM, Reissner's membrane; SG, spiral ganglion; SL, spiral ligament. Scale bars: $B = 0.2$ mm and also applies to *A*; $Fa = 20$ μm and also applies to *Ea*.

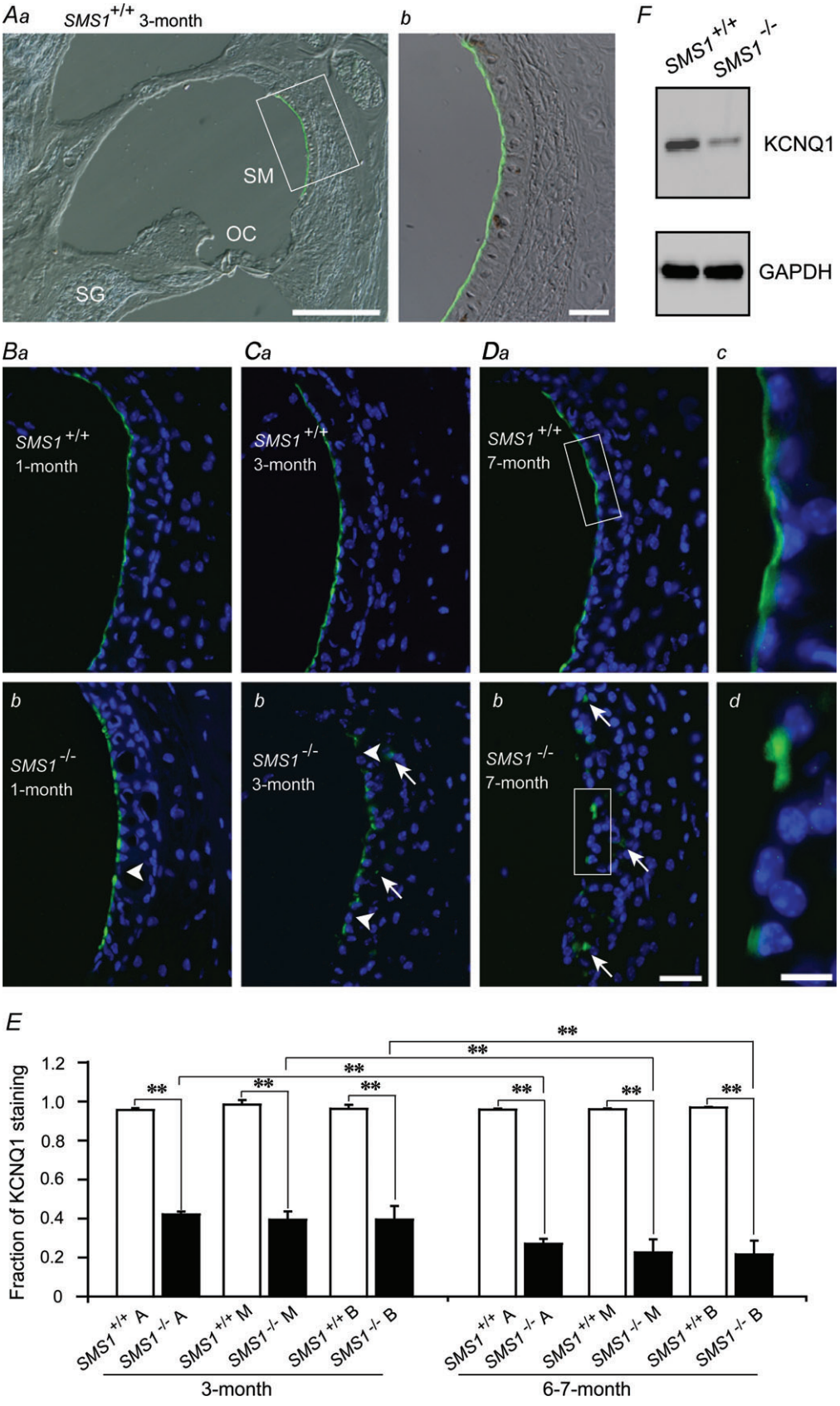

shows the staining pattern in a 1-month-old $SMS1^{+/+}$ mouse (Fig. 5*Ba*) and an age-matched $SMS1^{-/-}$ mouse (Fig. 5*Bb*). It is clear from the figure that while staining in the $SMS1^{+/+}$ mouse appeared rather continuous across the SV (Fig. 5*Ba*), some locations in the $SMS1^{-/-}$ mouse appeared to be deprived of staining (Fig. 5*Bb*, arrowhead). In 3-month-old $SMS1^{-/-}$ mice, more sites lacked staining (Fig. 5*Cc*, arrowheads). At this age, aberrant expression of the channel was also observed at locations other than the apical surface of marginal cells (Fig. 5*Cb*, arrows). In 7-month-old animals, the staining of KCNQ1 at the apical surface of $SMS1^{-/-}$ mouse marginal cells became only punctuate (Fig. 5*Db*, d), and aberrant expression within the parenchyma of the SV (Fig. 5*Db*, arrows) became comparable to that on the apical surface.

To examine cochlear location dependence and age dependence of KCNQ1 expression, we quantified the expression by measuring the fraction of KCNQ1-positive length along the SV surface. As shown in Fig. 5*E*, the fraction was close to one for all $SMS1^{+/+}$ mice, but was significantly reduced in $SMS1^{-/-}$ mice, at all cochlear locations. The results also revealed an age-dependent reduction at all cochlear locations (Fig. 5*E*). However, we found no significant difference *between* cochlear locations (Fig. 5*E*).

To quantify the protein level of KCNQ1 in the SV, we performed Western blot analysis. As shown in Fig. 5*F*, the expression of KCNQ1 in 3-month-old $SMS1^{-/-}$ mice was markedly reduced. The expression level of KCNQ1 in $SMS1^{-/-}$ mice, normalized to the level of GAPDH expression, was 60% of that in the age-matched controls (Fig. 5*F*).

Pigmentation in the SV

Although the above analyses shed some light on the mechanisms underlying hearing loss in $SMS1^{-/-}$ mice, the mechanism underlying the frequency dependence of hearing loss remains elusive. Our previous study of $SMS1^{-/-}$ mice demonstrated increased reactive oxygen species in these animals (Yano *et al.* 2011). In the cochlea, oxidative stress is known to induce macrophage invasion into the SV (Jabba *et al.* 2006, Singh & Wangemann, 2008). We thus examined macrophage invasion of the SV at different cochlear locations and at different ages. As shown in Fig. 6*A–D*, macrophages were visible in transmission images of the SV by their pigmentation (Jabba *et al.* 2006), and there appeared to be more pigmentation in the KO animals. We quantified macrophage invasion by calculating the ratio of the area of pigmentation to the area of the SV, and found a significant enhancement at the apical turn in $SMS1^{-/-}$ mice compared with $SMS1^{+/+}$ mice, but not at the basal turn, at 3 months of age (Fig. 6*E*). There was also a tendency for more pigmentation at the apical turn than the basal turn in KO animals, at both 3 months of age and 6–7 months of age (Fig. 6*E*).

Discussion

In the present study, we demonstrated for the first time that SMS1-dificiency caused hearing loss while SMS2-dificiency did not. We showed that the hearing loss in $SMS1^{-/-}$ mice occurred in a low frequency range and was progressive with age. The results also demonstrated abnormalities in the inner ear of $SMS1^{-/-}$ mice. Specifically, we found atrophy of the SV, disorganization of SV marginal cells, reduced EPs, altered expression of the potassium channel KCNQ1 in marginal cells, and a greater increase of macrophage invasion into the SV at the apical cochlea. In addition, a reduced level of DPOAE was observed in $SMS1^{-/-}$ mice compared with $SMS1^{+/+}$ controls.

Hearing loss in $SMS1^{-/-}$ mice, but not in $SMS2^{-/-}$ mice

An immediate question raised by our results is why hearing impairment was observed in $SMS1^{-/-}$ but not $SMS2^{-/-}$ mice. However, the explanation for this phenomenon is currently unclear. The results revealed that both SMS1 and SMS2 were expressed in the cochlea (see Fig. S1). Previous studies have also demonstrated the expression of both enzymes in the brain (Huitema *et al.* 2004; Yang *et al.* 2005), although the exact expression pattern of these enzymes in the auditory system is not known

Figure 5. Altered expression of KCNQ1 in the SV of $SMS1^{-/-}$ mice*Aa*, specific expression of KCNQ1 in the SV in a 3-month-old $SMS1^{+/+}$ mouse cochlear section. KCNQ1 immunofluorescence (green in the boxed area) was merged with a brightfield image of the section. *Ab*, an enlarged view of the boxed area in *Aa*. *B–D*, KCNQ1 immunostained SV sections of $SMS1^{+/+}$ (*Ba*, *Ca*, *Da* and *Dc*) and $SMS1^{-/-}$ (*Bb*, *Cb*, *Db* and *Dd*) mice at 1 (*B*), 3 (*C*) and 7 (*D*) months of age. *Dc* and *Dd* are enlarged versions of the boxed area in *Da* and *Db*, respectively. KCNQ1 signals (green) were merged with images of DAPI-stained cell nuclei (blue). *E*, fraction of KCNQ1 staining along the SV surface in $SMS1^{+/+}$ and $SMS1^{-/-}$ mice at 3 months of age ($n = 5$ for all genotypes) and at 6–7 months of age ($SMS1^{+/+}$, $n = 3$; $SMS1^{-/-}$, $n = 4$). A, M and B represent apical, middle and basal turn of the cochlea, respectively. *F*, Western blot analysis for quantification of the KCNQ1 expression level in 3-month-old mice. Scale bars: *Aa* = 0.2 mm; *Ab* = 30 μm; *Db* = 30 μm and applies also to *B*, *C* and *Da*; *Dd* = 10 μm and applies also to *Dc*.

at this time. It is known, however, that whereas SMS1 resides in the membrane of the Golgi apparatus, SMS2 is primarily found in the cytoplasmic membrane (Huitema *et al.* 2004; Tafesse *et al.* 2006; Mitsutake *et al.* 2011; Kidani *et al.* 2012). SM synthesis starts with the formation of ceramide in the endoplasmic reticulum, with ceramide being subsequently transported to the Golgi where SM is synthesized by SMS1. Furthermore, SM cycles between the Golgi and cytoplasmic membrane where SMS2 interconverts ceremide and SM (Tafesse *et al.* 2006). SMS1 thus appears to be essential to SM synthesis, whereas SMS2 plays only a regulatory role (Yamaoka *et al.* 2004). Such

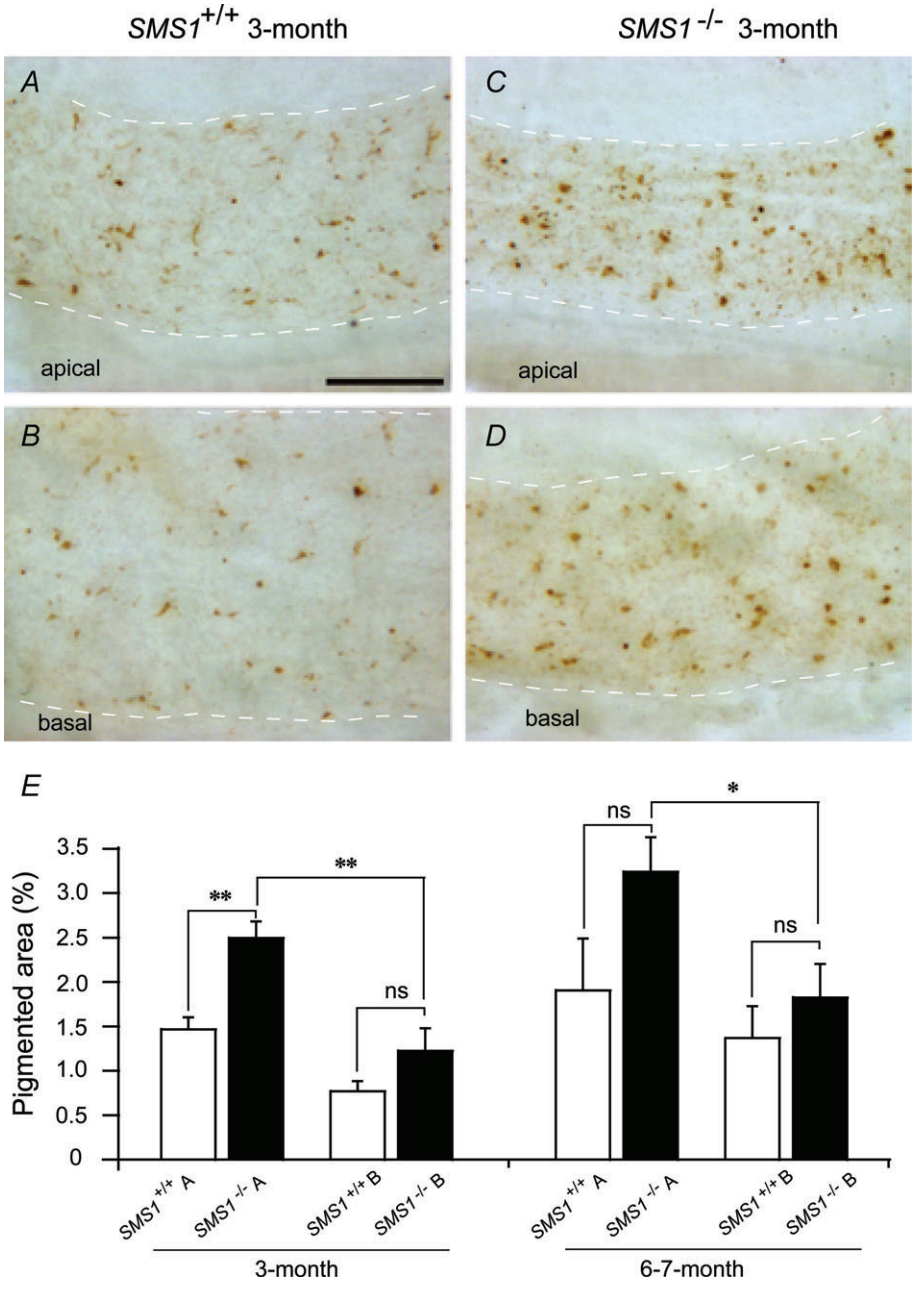

Figure 6. Increased pigmentation in the SV of *SMS1*$^{-/-}$ mice
A–D, brightfield microscope images of the SV in flat-mount cochlear lateral wall tissues, prepared from 3-month-old *SMS1*$^{+/+}$ (*A* and *B*) and *SMS1*$^{-/-}$ (*C* and *D*) mice at the apical (*A* and *C*) and basal (*B* and *D*) turn of the cochleae. The SV could be identified as a pigmented stripe (the area between the two dotted lines in each figure). Pigment was accumulated more in the *SMS1*$^{-/-}$ mice (*C* and *D*) than *SMS1*$^{+/+}$ mice (*A* and *B*). Scale bar: 0.2 mm. *E*, the percentage of pigmented area to the area of the SV at the apical (A) and basal (B) turns of cochleae in *SMS1*$^{+/+}$ and *SMS1*$^{-/-}$ mice, at 3 months of age ($n = 5$ for both genotypes) and 6–7 months of age (*SMS1*$^{+/+}$, $n = 5$; *SMS1*$^{-/-}$, $n = 4$).

differential roles of SMS1 and SMS2 and their differential subcellular localization should serve as clues for further investigating why different phenotypes of KO animals were observed here. Despite normal hearing ability, *SMS2*$^{-/-}$ animals were recently found to exhibit alterations both at the molecular and tissue level in a number of organs (Liu *et al.* 2009; Gowda *et al.* 2011; Li *et al.* 2011; Mitsutake *et al.* 2011; Zhang *et al.* 2011).

Features of the hearing impairment in *SMS1*$^{-/-}$ mice

The results revealed several characteristic features of the hearing impairment in *SMS1*$^{-/-}$ mice. First, the impairment was more prominent for low frequency tones. Second, compared with the hearing impairments in mice deficient in other lipid-related enzymes, the impairment in *SMS1*$^{-/-}$ mice was mild to moderate. For example, the largest increase in the ABR threshold in *SMS1*$^{-/-}$ mice was 40–50 dB, compared with the control mice (see Fig. 1). Mice genetically devoid of ganglioside synthase, in contrast, exhibit complete hearing loss (Yoshikawa *et al.* 2009). Third, the impairment was progressive with age. Evidence from ABR experiments, EP recordings, and KCNQ1 staining all suggests an age-dependent progression of hearing impairment in *SMS1*$^{-/-}$ mice.

It is now well known that a mutation of the *cadherin 23* gene (*Cdh23*), increases the susceptibility of early onset of age-related hearing loss (Noben-Trauth *et al.* 2003). Our SMS1- and SMS2-KO mice were generated using D3 stem cells, which originate from a 129 substrain, backcrossed with the C57BL/6 strain; both strains carry the *Cdh23ahl* allele (Noben-Trauth *et al.* 2003). Thus a possible effect of *Cdh23ahl* allele on the early onset and progressive nature of the hearing loss in *SMS1*$^{-/-}$ mice must be considered. Among cochlear cell types, hair cells and cells of the Reissner's membrane are known to express Cdh23 (Lagziel *et al.* 2005; Rzadzinska *et al.* 2005), raising the possibility of interaction between SMS1 and Cdh23 in these cells. Nevertheless, for the following reasons, the hearing loss we observed in *SMS1*$^{-/-}$ mice appears primarily attributable to SMS1 deficiency. First, the hearing loss in *SMS1*$^{-/-}$ mice was observed by comparison with *SMS1*$^{+/+}$ controls. Second, *Cdh23ahl* allele-related hearing loss occurs in high frequency ranges (Kane *et al.* 2012), in contrast to the hearing loss in low frequency ranges in *SMS1*$^{-/-}$ mice observed here. Third, *Cdh23ahl* allele-related hearing loss is caused by a loss of hair cells (Kane *et al.* 2012), but here we observed no significant difference in hair cell loss between *SMS1*$^{-/-}$ and *SMS1*$^{+/+}$ mice. Rather, abnormalities in the SV of *SMS1*$^{-/-}$ mice appeared to be the primary mechanism for hearing loss. Finally, *Cdh23ahl* allele-related hearing loss starts from approximately 3 months after birth (Kane *et al.* 2012), but hearing loss in *SMS1*$^{-/-}$ mice was observed here from the first month.

Mechanisms for hearing loss in *SMS1*$^{-/-}$ mice

Our results suggest that atrophy of the SV may, at least in part, account for the hearing impairment in *SMS1*$^{-/-}$ mice. Reduction of the width of the SV and the disorganization of the marginal cells may all result in the attenuated EPs observed in these animals. EPs add to the driving force for K^+ ions to enter hair cells through mechanoelectrical transduction channels that are activated upon acoustic stimulation. Loss of the EP thus reduces the sensitivity of hair cells to sound stimulation and leads to hearing impairment. The observation that the progressive reduction in the EPs paralleled the ABR threshold elevation (compare Fig. 2*C* to Fig. 1*B*) also supports a causal role for EP attenuation in the hearing loss of *SMS1*$^{-/-}$ mice.

To explore the mechanisms for the attenuated EPs in *SMS1*$^{-/-}$ mice, we measured endocochlear K^+ concentrations, but found no significant changes. Instead, we found that KCNQ1 channels, which are normally expressed on the apical membrane of all SV marginal cells, were not expressed in some cells that faced the scala media in *SMS1*$^{-/-}$ mice. Moreover, in these mice, aberrant expression of KCNQ1 was found in the parenchyma of the SV, presumably on the processes of marginal cells within the SV. At the tissue level, the expression level of KCNQ1 was also low in *SMS1*$^{-/-}$ mice. KCNQ1 normally passes K^+ from the cytoplasm of marginal cells to the endolymph (Wangemann, 2002; Hibino *et al.* 2010). The major component of the EP is created by the low K^+ concentration in the intrastrial space, the extracellular space confined by the two epithelial barriers of marginal cells and basal cells of the SV, both of which are formed by cells interconnected with tight junctions (Wangemann, 2002; Kitajiri *et al.* 2004; Hibino *et al.* 2010). The K^+ concentration in the intrastrial space is regulated by ion channels, pumps, exchangers, and transporters of both the marginal cells and the basal cells (Wangemann, 2002; Hibino *et al.* 2010). Aberrant and reduced expression of KCNQ1 in the marginal cells of *SMS1*$^{-/-}$ mice may have caused an increase of K^+ concentration in the intrastrial space, leading to attenuation of EPs. Hearing impairments resulting from the loss of KCNQ1 channels in SV have also been previously reported in mice deficient in the lysosomal membrane protein LIMP2 (Knipper *et al.* 2006), and mutations in the gene encoding KCNQ1 α-subunit have been shown to cause deafness (Neyroud *et al.* 1997).

It remains unclear whether the attenuation of the EP is cochlear location dependent, and whether it explains the frequency dependence of hearing loss in *SMS1*$^{-/-}$ mice. We measured EPs from only one site in the endolymph because the mouse cochlea is too small to allow

measurement at different locations. EPs are determined not only by KCNQ1 channels; other channels such as KCNJ10 and the Na^+/K^+ pump also play essential roles in creating the potential (Wangemann, 2002; Hibino *et al.* 2010). Previous studies have demonstrated oxidative stress-induced loss of KCNJ10 in the SV (Jabba *et al.* 2006; Singh & Wangemann, 2008). In light of the current observation that the apical region of *SMS1*$^{-/-}$ mouse cochleae was more invaded by macrophages than the basal region (see Fig. 6), it is possible that the expression of EP-related molecules other than KCNQ1 but including KCNJ10, Cl^- channels and Cl^- transporters (Rickheit *et al.* 2008) is altered more in the apical region and causes a greater drop in the EP.

To explore the mechanisms underlying the frequency dependence of the hearing impairment, we measured DPOAE. However, DPOAE in the *SMS1*$^{-/-}$ mice was found to be reduced at a middle frequency range of 8–16 kHz. DPOAE is a non-linear phenomenon, thought to be produced by active processes within the cochlea. Recent evidence suggests that it can be attributed to the somatic motor of outer hair cells and the hair bundle motor of both inner and outer hair cells (for reviews see Dallos & Fakler 2002, Kemp 2002, Fettiplace & Hackney 2006, and Ashmore 2008), with the prestin protein and mechanoelectrical transduction channels playing key roles in the somatic motor and hair bundle motor, respectively. Although our DPOAE results do not fully explain the frequency dependence of hearing loss in *SMS1*$^{-/-}$ mice (in particular the hearing loss at 4 kHz and 6 kHz judging from the ABR results), the results do suggest functional impairment of outer/inner hair cells in these mice. The fact that our DPOAE results cannot fully explain the frequency dependence of hearing loss in the *SMS1*$^{-/-}$ mice suggests that there may be additional impairments of the apical region of the cochleae in these mice. Such impairment might be caused by oxidative stress, considering our observation that macrophage density was more enhanced in the apical region than the basal region in *SMS1*$^{-/-}$ mice.

Another feature of the hearing impairment in *SMS1*$^{-/-}$ mice is its age-dependent progression. It is widely known that age-dependent development of hearing loss occurs in wild-type animals. However, in the current study hearing loss had an early onset and was accelerated in *SMS1*$^{-/-}$ mice compared with *SMS1*$^{+/+}$ controls (see Fig. 1*B*). The mechanism for age-dependent hearing loss is at least partially attributable to oxidative stress that impairs cell function or induces cell death (Staecker *et al.* 2001; Jiang *et al.* 2007). We have recently shown that mice genetically devoid of SMS1 exhibited increased reactive oxygen species (Yano *et al.* 2011). Although we found no obvious cell loss in the *SMS1*$^{-/-}$ mouse cochleae up to an age of 7 months, the accelerated progression of hearing loss in these mice may have been caused by increased oxidative stress. This notion is consistent with our observation that macrophage density in *SMS1*$^{-/-}$ mouse cochleae tended to be higher than in *SMS1*$^{+/+}$ controls.

In summary, our results show for the first time that SMS1 but not SMS2 is involved in hearing, and that SMS1 deficiency causes progressive hearing loss at a low frequency range. Our results show an essential role of SMS1 for SV homeostasis, and suggest the involvement of an SMS1-related pathway in the regulation of the SV KCNQ1 channel. Future studies should elucidate the mechanisms underlying the differential roles of SMS1 and SMS2 in hearing, and examine the link between SM metabolism and frequency-dependent hearing at the molecular level.

References

Ashmore J (2008). Cochlear outer hair cell motility. *Physiol Rev* **88**, 173–210.

Dallos P & Fakler B (2002). Prestin, a new type of motor protein. *Nat Rev Mol Cell Biol* **3**, 104–111.

Darios F, Wasser C, Shakirzyanova A, Giniatullin A, Goodman K, Munoz-Bravo JL, Raingo J, Jorgacevski J, Kreft M, Zorec R, Rosa JM, Gandia L, Gutiérrez LM, Binz T, Giniatullin R, Kavalali ET & Davletov B (2009). Sphingosine facilitates SNARE complex assembly and activates synaptic vesicle exocytosis. *Neuron* **62**, 683–694.

Dong L, Watanabe K, Itoh M, Huan CR, Tong XP, Nakamura T, Miki M, Iwao H, Nakajima A, Sakai T, Kawanami T, Sawaki T, Masaki Y, Fukushima T, Fujita Y, Tanaka M, Yano M, Okazaki T & Umehara H (2012). CD4+ T-cell dysfunctions through the impaired lipid rafts ameliorate concanavalin A-induced hepatitis in sphingomyelin synthase 1-knockout mice. *Int Immunol* **24**, 327–337.

Dunbar GL, Lescaudron LL & Stein DG (1993). Comparison of GM1 ganglioside, AGF2, and D-amphetamine as treatments for spatial reversal and place learning deficits following lesions of the neostriatum. *Behav Brain Res* **54**, 67–79.

Fettiplace R & Hackney CM (2006). The sensory and motor roles of auditory hair cells. *Nat Rev Neurosci* **7**, 19–29.

Gowda S, Yeang C, Wadgaonkar S, Anjum F, Grinkina N, Cutaia M, Jiang XC & Wadgaonkar R (2011). Sphingomyelin synthase 2 (SMS2) deficiency attenuates LPS-induced lung injury. *Am J Physiol Lung Cell Mol Physiol* **300**, L430–440.

Hannun YA & Obeid LM (2002). The Ceramide-centric universe of lipid-mediated cell regulation: stress encounters of the lipid kind. *J Biol Chem* **277**, 25847–25850.

Herr DR, Grillet N, Schwander M, Rivera R, Müller U & Chun J (2007). Sphingosine 1-phosphate (S1P) signaling is required for maintenance of hair cells mainly via activation of S1P2. *J Neurosci* **27**, 1474–1478.

Hibino H, Nin F, Tsuzuki C & Kurachi Y (2010). How is the highly positive endocochlear potential formed? The specific architecture of the stria vascularis and the roles of the ion-transport apparatus. *Pflugers Arch* **459**, 521–533.

Huitema K, van den Dikkenberg J, Brouwers JF & Holthuis JC (2004). Identification of a family of animal sphingomyelin synthases. *EMBO J* **23**, 33–44.

Inokuchi J, Mizutani A, Jimbo M, Usuki S, Yamagishi K, Mochizuki H, Muramoto K, Kobayashi K, Kuroda Y, Iwasaki K, Ohgami Y & Fujiwara M (1997). Up-regulation of ganglioside biosynthesis, functional synapse formation, and memory retention by a synthetic ceramide analog (L-PDMP). *Biochem Biophys Res Commun* **237**, 595–600.

Jabba SV, Oelke A, Singh R, Maganti RJ, Fleming S, Wall SM, Everett LA, Green ED & Wangemann P (2006). Macrophage invasion contributes to degeneration of stria vascularis in Pendred syndrome mouse model. *BMC Med* **4**, 37.

Jiang H, Talaska AE, Schacht J & Sha SH (2007). Oxidative imbalance in the aging inner ear. *Neurobiol Aging* **28**, 1605–1612.

Jung SY, Suh JH, Park HJ, Jung KM, Kim MY, Na DS & Kim DK (2000). Identification of multiple forms of membrane-associated neutral sphingomyelinase in bovine brain. *J Neurochem* **75**, 1004–1014.

Kane KL, Longo-Guess CM, Gagnon LH, Ding D, Salvi RJ & Johnson KR (2012). Genetic background effects on age-related hearing loss associated with Cdh23 variants in mice. Hear Res. 283, 80–88.

Kemp DT (2002). Otoacoustic emissions, their origin in cochlear function, and use. *Br Med Bull* **63**, 223–241.

Kidani Y, Ohshima K, Sakai H, Kohno T, Baba A & Hattori M (2012). Differential localization of sphingomyelin synthase isoforms in neurons regulates sphingomyelin cluster formation. *Biochem Biophys Res Commun* **417**, 1014–1017.

Kitajiri S, Miyamoto T, Mineharu A, Sonoda N, Furuse K, Hata M, Sasaki H, Mori Y, Kubota T, Ito J, Furuse M & Tsukita S (2004). Compartmentalization established by claudin-11-based tight junctions in stria vascularis is required for hearing through generation of endocochlear potential. *J Cell Sci* **117**, 5087–5096.

Knipper M, Claussen C, Rüttiger L, Zimmermann U, Lüllmann-Rauch R, Eskelinen EL, Schröder J, Schwake M & Saftig P (2006). Deafness in LIMP2-deficient mice due to early loss of the potassium channel KCNQ1/KCNE1 in marginal cells of the stria vascularis. *J Physiol* **576**, 73–86.

Konagaya M, Konishi T, Konagaya Y, Takayanagi T, Kita E & Muto T (1989). Partial sphingomyelinase deficiency with sea-blue histiocytosis and neurovisceral dysfunction. *Jpn J Med* **28**, 85–88.

Kono M, Belyantseva IA, Skoura A, Frolenkov GI, Starost MF, Dreier JL, Lidington D, Bolz SS, Friedman TB, Hla T & Proia RL (2007). Deafness and stria vascularis defects in S1P2 receptor-null mice. *J Biol Chem* **282**, 10690–10696.

Lagziel A, Ahmed ZM, Schultz JM, Morell RJ, Belyantseva IA & Friedman TB (2005). Spatiotemporal pattern and isoforms of cadherin 23 in wild type and waltzer mice during inner ear hair cell development. *Dev Biol* **280**, 295–306.

Li Z, Zhang H, Liu J, Liang CP, Li Y, Li Y, Teitelman G, Beyer T, Bui HH, Peake DA, Zhang Y, Sanders PE, Kuo MS, Park TS, Cao G & Jiang XC (2011). Reducing plasma membrane sphingomyelin increases insulin sensitivity. *Mol Cell Biol* **31**, 4205–4218.

Liu J, Huan C, Chakraborty M, Zhang H, Lu D, Kuo MS, Cao G & Jiang XC (2009). Macrophage sphingomyelin synthase 2 deficiency decreases atherosclerosis in mice. *Circ Res* **105**, 295–303.

MacLennan AJ, Benner SJ, Andringa A, Chaves AH, Rosing JL, Vesey R, Karpman AM, Cronier SA, Lee N, Erway LC & Miller ML (2006). The $S1P_2$ sphingosine 1-phosphate receptor is essential for auditory and vestibular function. *Hear Res* **220**, 38–48.

Merrill AH Jr (2002). De novo sphingolipid biosynthesis: a necessary, but dangerous, pathway. *J Biol Chem* **277**, 25843–25846.

Mihaylova V, Hantke J, Sinigerska I, Cherninkova S, Raicheva M, Bouwer S, Tincheva R, Khuyomdziev D, Bertranpetit J, Chandler D, Angelicheva D, Kremensky I, Seeman P, Tournev I & Kalaydjieva L (2007). Highly variable neural involvement in sphingomyelinase-deficient Niemann-Pick disease caused by an ancestral Gypsy mutation. *Brain* **130**, 1050–1061.

Mitsutake S, Zama K, Yokota H, Yoshida T, Tanaka M, Mitsui M, Ikawa M, Okabe M, Tanaka Y, Yamashita T, Takemoto H, Okazaki T, Watanabe K & Igarashi Y (2011). Dynamic modification of sphingomyelin in lipid microdomains controls development of obesity, fatty liver, and type 2 diabetes. *J Biol Chem* **286**, 28544–28555.

Müller M, von Hünerbein K, Hoidis S & Smolders JW (2005). A physiological place-frequency map of the cochlea in the CBA/J mouse. *Hear Res* **202**, 63–73.

Neyroud N, Tesson F, Denjoy I, Leibovici M, Donger C, Barhanin J, Fauré S, Gary F, Coumel P, Petit C, Schwartz K & Guicheney P (1997). A novel mutation in the potassium channel gene KVLQT1 causes the Jervell and Lange-Nielsen cardioauditory syndrome. *Nat Genet* **15**, 186–189.

Nin F, Hibino H, Doi K, Suzuki T, Hisa Y & Kurachi Y (2008). The endocochlear potential depends on two K^+ diffusion potentials and an electrical barrierin the stria vascularis of the inner ear. *Proc Natl Acad Sci U S A* **105**, 1751–1756.

Nishimura M, Shirasawa H, Kaizo H & Song W-J (2007). New field with tonotopic organization in Guinea pig auditory cortex. *J Neurophysiol* **97**, 927–932.

Noben-Trauth K, Zheng QY & Johnson KR (2003). Association of cadherin 23 with polygenic inheritance and genetic modification of sensorineural hearing loss. *Nat Genet* **35**, 21–23.

Polesskaya O, Cunningham LL, Francis SP, Luebke AE, Zhu X, Collins D, Vasilyeva ON, Sahler J, Desmet EA, Gelbard HA, Maggirwar SB, Walton JP, Frisina RD Jr & Dewhurst S (2010). Ablation of mixed lineage kinase 3 (Mlk3) does not inhibit ototoxicity induced by acoustic trauma or aminoglycoside exposure. *Hear Res* **270**, 21–27.

Rickheit G, Maier H, Strenzke N, Andreescu CE, De Zeeuw CI, Muenscher A, Zdebik AA & Jentsch TJ (2008). Endocochlear potential depends on Cl^- channels: mechanism underlying deafness in Bartter syndrome IV. *EMBO J* **27**, 2907–2917.

Rzadzinska AK, Derr A, Kachar B & Noben-Trauth K (2005). Sustained cadherin 23 expression in young and adult cochlea of normal and hearing-impaired mice. *Hear Res* **208**, 114–121.

Sakagami M, Fukazawa K, Matsunaga T, Fujita H, Mori N, Takumi T, Ohkubo H & Nakanishi S (1991). Cellular localization of rat Isk protein in the stria vascularis by immunohistochemical observation. *Hear Res* **56**, 168–172.

Singh R & Wangemann P (2008). Free radical stress-mediated loss of Kcnj10 protein expression in stria vascularis contributes to deafness in Pendred syndrome mouse model. *Am J Physiol Renal Physiol* **294**, F139–148.

Spiegel S & Milstien S (2002). Sphingosine 1-phosphate, a key cell signaling molecule. *J Biol Chem* **277**, 25851–25854.

Staecker H, Zheng QY & Van De Water TR (2001). Oxidative stress in aging in the C57B16/J mouse cochlea. *Acta Otolaryngol* **121**, 666–672.

Tafesse FG, Ternes P & Holthuis JC (2006). The multigenic sphingomyelin synthase family. *J Biol Chem* **281**, 29421–29425.

Wangemann P (2002). K^+ cycling and the endocochlear potential. *Hear Res* **165**, 1–9.

Xu Y, Ramu Y & Lu Z (2008). Removal of phospho-head groups of membrane lipids immobilizes voltage sensors of K^+ channels. *Nature* **451**, 826–829.

Yamagata K, Senokuchi T, Lu M, Takemoto M, Fazlul Karim M, Go C, Sato Y, Hatta M, Yoshizawa T, Araki E, Miyazaki J & Song WJ (2011). Voltage-gated K^+ channel KCNQ1 regulates insulin secretion in MIN6 beta-cell line. *Biochem Biophys Res Commun* **407**, 620–625.

Yamaoka S, Miyaji M, Kitano T, Umehara H & Okazaki T (2004). Expression cloning of a human cDNA restoring sphingomyelin synthesis and cell growth in sphingomyelin synthase-defective lymphoid cells. *J Biol Chem* **279**, 18688–18693.

Yano M, Watanabe K, Yamamoto T, Ikeda K, Senokuchi T, Lu M, Kadomatsu T, Tsukano H, Ikawa M, Okabe M, Yamaoka S, Okazaki T, Umehara H, Gotoh T, Song WJ, Node K, Taguchi R, Yamagata K & Oike Y (2011). Mitochondrial dysfunction and increased reactive oxygen species impair insulin secretion in sphingomyelin synthase 1-null mice. *J Biol Chem* **286**, 3992–4002.

Yang Z, Jean-Baptiste G, Khoury C & Greenwood MT (2005). The mouse sphingomyelin synthase 1 (SMS1) gene is alternatively spliced to yield multiple transcripts and proteins. *Gene* **363**, 123–132.

Yoshikawa M, Go S, Takasaki K, Kakazu Y, Ohashi M, Nagafuku M, Kabayama K, Sekimoto J, Suzuki S, Takaiwa K, Kimitsuki T, Matsumoto N, Komune S, Kamei D, Saito M, Fujiwara M, Iwasaki K & Inokuchi J (2009). Mice lacking ganglioside GM3 synthase exhibit complete hearing loss due to selective degeneration of the organ of Corti. *Proc Natl Acad Sci U S A* **106**, 9483–9488.

Zhang Y, Dong J, Zhu X, Wang W & Yang Q (2011). The effect of sphingomyelin synthase 2 (SMS2) deficiency on the expression of drug transporters in mouse brain. *Biochem Pharmacol* **82**, 287–294.

Author contributions

M.H.L., M.T., H.L., and M.N. carried out the experiment and analyzed the data; K.W., M.Y., H.T., T.O. and Y.O. made the KO mice; W.J.S. conceived the experiment and wrote the paper. All Authors approved the final version.

Acknowledgements

We thank Drs H. Hibino and S. Yamaguchi for advice on K^+ concentration measurement, Dr P. Narins for advice on DPOAE measurement, Dr K. Yamagata for advice on Western blotting, Dr F. Murakami for support and discussion, and the Gene Technology Center in Kumamoto University for use of their equipment. This work was supported by a Grant-in-Aid for Scientific Research on Innovative Areas 'Mesoscopic Neurocircuitry' (no. 23115516) of The Ministry of Education, Science, Sports and Culture of Japan and grants from Japan Society for the Promotion of Science (nos 20300112, 22220004 and 23659797), and in part by the scholarship for the Graduate School of Medical Sciences, Kumamoto University.